ORIGINAL ARTICLE

Release mechanism of micrometer-scale particles from transient networks with well-controlled structures

Sayuri Tanaka[1] · Kyohhei Fujita[2] · Yuta Yamamoto[1] · Farah Aqilah Md Zulkiflie[1] · Taichi Suzuki[1] · Mitsuru Naito [3] · Ung-il Chung[1,4] · Takuya Katashima [1]

Abstract

Practical applications of viral- and cell-based therapeutics require precise targeted delivery to minimize off-target effects. Conventional hydrogel-based drug delivery carriers may undergo a sol–gel phase transition upon in vivo degradation, leading to a burst release of encapsulated substances. Transient-network materials have been proposed to overcome this challenge. However, the relationship between the network structure and release mechanisms remains unclear, mainly due to the lack of control over structural heterogeneity in typical transient networks. This study aimed to elucidate the mechanism underlying the release of micrometer-scale particles from transient networks using a systematically controlled model system composed of tetra-armed polyethylene glycol (Tetra-PEG slime). The system features a well-defined structure with uniform strand lengths and consistent functionalities. Our results demonstrate that particle release is driven by the dissolution of the matrix and that the release barrier depends on the surrounding network topology. This release behavior is primarily determined by network connectivity and is independent of the polymer concentration and strand length. These insights advance our understanding of the sustainable release of microparticles from transient networks and provide broadly applicable guidelines for the development of effective drug delivery systems.

Introduction

In recent years, significant advancements have been made in diversifying drug modalities. In addition to small-molecule drugs and biopharmaceuticals, therapeutics based on cells and viruses have been developed. Cell therapy involves the transfer of specific cell types (i.e., stem cells [1], chimeric antigen receptor T cells [2], dendritic cells [3], etc.) into the body to treat or prevent a disease. This approach leverages the unique properties of cells to repair, replace, or enhance the biological functions of damaged tissues or organs. Similarly, viral therapy converts viruses into therapeutic agents by reprogramming them to treat diseases. Adeno-associated viruses are potent tools for gene transduction and have been widely used in clinical practice. Although the use of higher doses results in a stronger effect, most of these cells or viruses accumulate in the liver, potentially causing local and systemic toxicity [4]. Therefore, minimizing off-target effects is highly important for the development of these therapeutics. Clinical cells and viruses vary in size, ranging from a few tens of nanometers to several micrometers; thus, they can easily circulate throughout the body, leading to unintended infections or adverse effects in undesired locations [5]. One major cause of off-target effects is the lack of effective methods to control the localization and release of cells and viruses, which can be approximated as particles on the micrometer scale. To address this, a variety of hydrogels have been developed [6–8].

Hydrogels are 3-dimensional polymer networks that absorb water while remaining insoluble in aqueous solutions. They are expected to trap substances within their irreversibly crosslinked networks, which are approximately ten nanometers in size, and release them slowly. However, in practical in vivo applications, hydrogels degrade over time due to hydrolysis and biological interactions, ultimately transitioning to a sol phase. At this point, their ability to trap substances drastically decreases, resulting in burst release [9, 10]. The significant change in release behavior near the transition zone is an unavoidable phenomenon observed in all hydrogels [11, 12]. To address this challenge, the use of transient network materials has been proposed. Transient networks are 3D structures formed by reversible crosslinks such as coordinate bonds, hydrophobic interactions, ionic bonds, and entanglements. Owing to the temporary nature of these crosslinks, transient networks exhibit an elastic response over a short timescale but are capable of flowing over longer durations, which categorizes them as viscoelastic liquid materials. Like hydrogels, these transient networks can trap active substances; however, unlike hydrogels, they are expected to dissolve gradually, enabling controlled release [13, 14].

Conventional transient networks have heterogeneous network structures consisting of static and dynamic components [15–17]. Static heterogeneity refers to structural defects in an equilibrium state, including dangling chains, loop structures, and the polydispersity of network strand lengths and functionalities. In contrast, dynamic heterogeneity often involves the coexistence of slow and fast dynamics, which are related to both the network component and the unimer and micelle components. Generally, these heterogeneous structures are uncontrollable and cannot be quantitatively assessed, hindering our understanding of the relationships between network structures and release properties.

Recently, we reported a model transient network system with well-controlled structures (known as Tetra-PEG slime) [18–20]. In the model system, 2 types of multiarmed polyethylene glycols (PEGs) are modified at their ends with phenylboronic acid and diols, which form dynamic covalent bonds in aqueous environments [21–24]. These precursors are synthesized with a narrow molar mass distribution, which promotes the formation of a regular network with a uniform strand length and functionality, significantly reducing static heterogeneity. Compared with traditional systems, the symmetric design of mutually associative precursors with similar mobilities minimizes micelle formation and reduces dynamic heterogeneity. Network connectivity (p), which is related to the dangling chain fraction, is dependent on the equilibrium constant (K) and the crosslink density, indicating a strong relationship between p and other network parameters, such as concentration and strand length. Several studies have focused on adjusting K by altering the chemical species or pH of a solvent [22, 23]. However, a change in hydrophobicity is frequently accompanied by the tuning of chemical species [25]. Owing to a significant change in K, the latter method cannot precisely control K near the pKa value. Consequently, none of the methods can achieve continuous and robust control over p. Therefore, the greatest advantage of Tetra-PEG slime is that it can control only p.

In this study, we employed Tetra-PEG slimes with systematically controlled network connectivity, concentration, and strand length to elucidate the release mechanism of microparticles from transient networks. These findings will advance our understanding of sustained microparticle release from transient network materials, providing broadly applicable guidelines for their use as drug carriers.

Experimental section

Sample preparation

Tetra-armed PEGs, in which the end groups were modified with 4-carboxy-3-fluorophenylboronic acid (FPBA) and D-(+)-glucose-1,5-lactone (GDL) (denoted as tetra-PEG-FPBA and tetra-PEG-GDL, respectively), were purchased from SINOPEG BIOTECH Co., Ltd. (Xiamen, China). The weight-average molar masses of these compounds were 10, 20, and 40×10^3 g mol^{-1}, corresponding to molar masses of the resultant network strands (M_s) of 5, 10, and 20×10^3 g mol^{-1}, respectively. Tetra-PEG slimes were prepared by dissolving tetra-PEG-FPBA and tetra-PEG-GDL in a phosphate buffer (pH 7.4, 200 mM) with polymer concentrations (c_{poly}) varying from 40 to 120 g L^{-1}. The slimes were formed by mixing the 2 precursor solutions in stoichiometric ratios (s), where s represents the fraction of the tetra-PEG molecules bearing GDL end groups to the total number of tetra-PEG molecules. The mixtures were allowed to react at 25 °C overnight. The fluorescent particles encapsulated in the Tetra-PEG slimes were fluorescently labeled polystyrene microspheres (Fluoresbrite® YG Microspheres, 2.5×10^{-2} g L^{-1}, 0.1 and 1 μm diameter; Polysciences, Inc.).

Release behavior of particles encapsulated in Tetra-PEG slimes

To investigate the release behavior of the particles, a solution of fluorescently labeled polystyrene particles at a concentration of 1.0 vol.% was combined with the polymer solution at a specific concentration to prepare Tetra-PEG slime-containing fluorescent particles. The release model was designed with a culture insert (pore size of 8.0 μm;

Sterile; Merck, Inc.) placed in a 12-well culture plate (Falcon® low-evaporation, flat-bottom tissue culture plates; Fisher Scientific, Pittsburgh, PA, USA).

A certain weight of the Tetra-PEG slime containing fluorescent particles was prepared on the insert and incubated at 25 °C for 24 h. The initial sample weight ranged from 50–150 mg. In our experimental setup, the slime completely spread to the bottom surface of the insert; therefore, the surface area through which the particles were released remained constant throughout the experiment. Subsequently, 2.5 mL of phosphate buffer was added to the well plate. The system was maintained at room temperature in the dark, and 1.25 mL of the release medium was collected from the plate at each time point to evaluate the concentration of the permeated substances. Following sampling, an equal volume of fresh phosphate buffer was added to maintain a constant total volume. The concentration of released particles was determined by measuring the fluorescence intensity ($\lambda_{ex} = 355$ nm, $\lambda_{em} = 460$ nm) using a plate reader (ARVO X3, Perkin–Elmer, Turku, Finland). Notably, the ionic strength of the outer solution (pH 7.4) was maintained at 200 mM in all the experiments to minimize the influence of ionic diffusion, thereby enabling the evaluation of release characteristics under controlled and consistent conditions.

Results and discussion

Figure 1 shows the angular frequency dependence of the storage and loss moduli (G' and G'', respectively) for the Tetra-PEG slime ($c = 60$ g L^{-1}, $M = 20,000$ g mol^{-1}, and $s = 0.50$) and the Tetra-PEG slime with particles ($c = 60$ g L^{-1}, $M = 20,000$ g mol^{-1}, $s = 0.50$, and concentration of particles $= 1.0$ vol.%). We employed 1 μm fluorescent polystyrene particles, which mimic cells and viruses around that size. Both spectra agreed well with each other, indicating that the effect of particle addition was negligible. Figure 2 shows the particle fraction collected from the outer buffer at different time points, where $F(t)$ is the fluorescence intensity at time t and F_{max} is the maximum fluorescence intensity after complete particle diffusion. The slope of $F(t)/F_{max}$ decreased with increasing initial mass of the Tetra-PEG slime. Figure 3A illustrates the time-dependent residual fraction ($R(t)$) in the insert and is calculated as $1 - F(t)/F_{max}$. The linear decrease in $R(t)$ with increasing time suggests that the particle release dynamics follow the relationship described by Eq. (1).

$$R(t) = 1 - k_{app}t \qquad (1)$$

where k_{app} is the apparent release rate constant.

Figure 3B shows the correlation between k_{app} and the initial mass of the Tetra-PEG slime (w_0), indicating that k_{app}
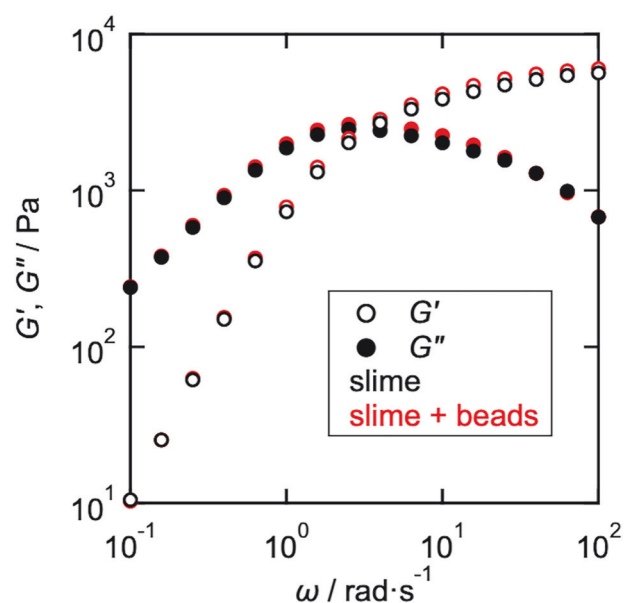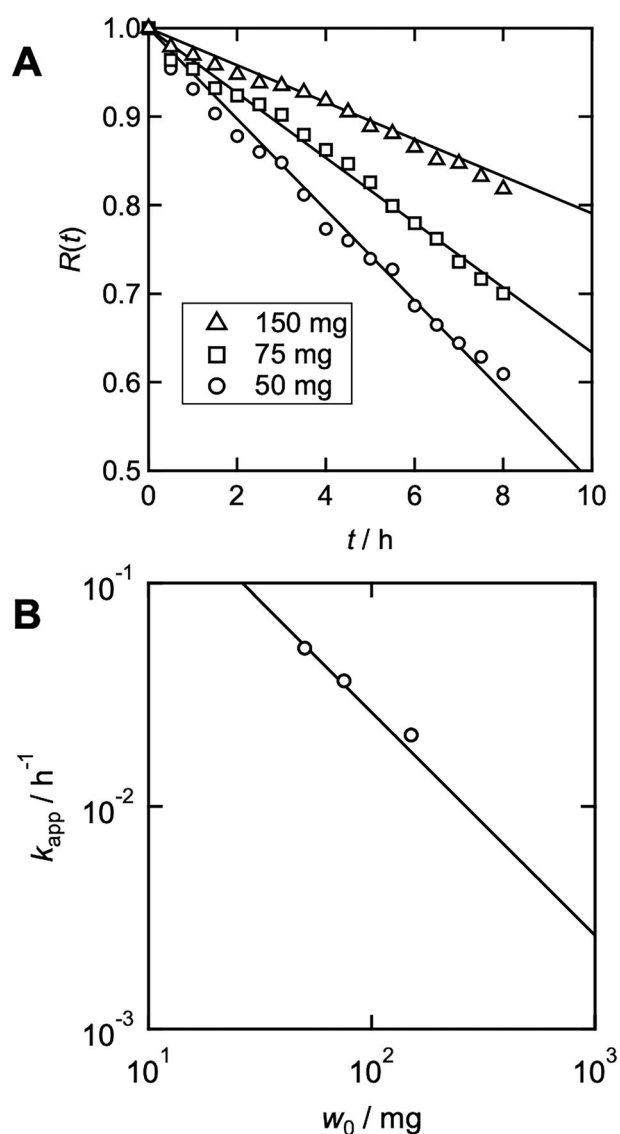

Fig. 1 Frequency dependence of the storage and loss moduli of Tetra-PEG slime. The black symbols represent the neat Tetra-PEG slime, and the red symbols represent the Tetra-PEG slime containing microparticles. The open and filled symbols represent G' and G'', respectively. Measurements were conducted at 25 °C. The solid lines indicate the predictions of the Maxwellian model
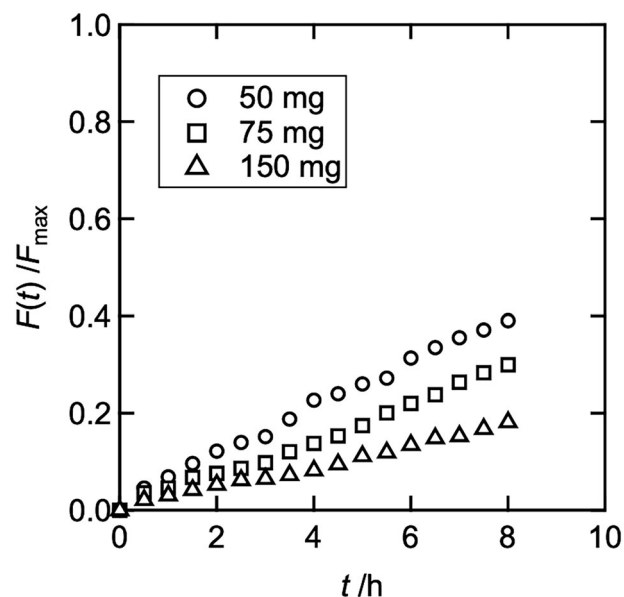
Fig. 2 Release profiles of the fluorescent particles from the Tetra-PEG slimes with different initial masses (circles: 50 mg, squares: 75 mg, and triangles: 150 mg)

follows a power-law relationship with w_0^{-1}, as represented by the solid line. This behavior aligns with the theoretical model proposed by Siepmann et al. [26, 27], which describes the kinetics of drug release and polymer dissolution from matrices composed of entangled polymer networks. Upon immersion of the matrix in water, the

the surface area through which the particles were released constant throughout the experiment. The time-dependent residual fraction $R(t)$, introduced in Eq. (1), can be expressed by Eq. (3).

$$R(t) = \frac{w_t}{w_0} = 1 - k \cdot A \cdot w_0^{-1} \cdot t \tag{3}$$
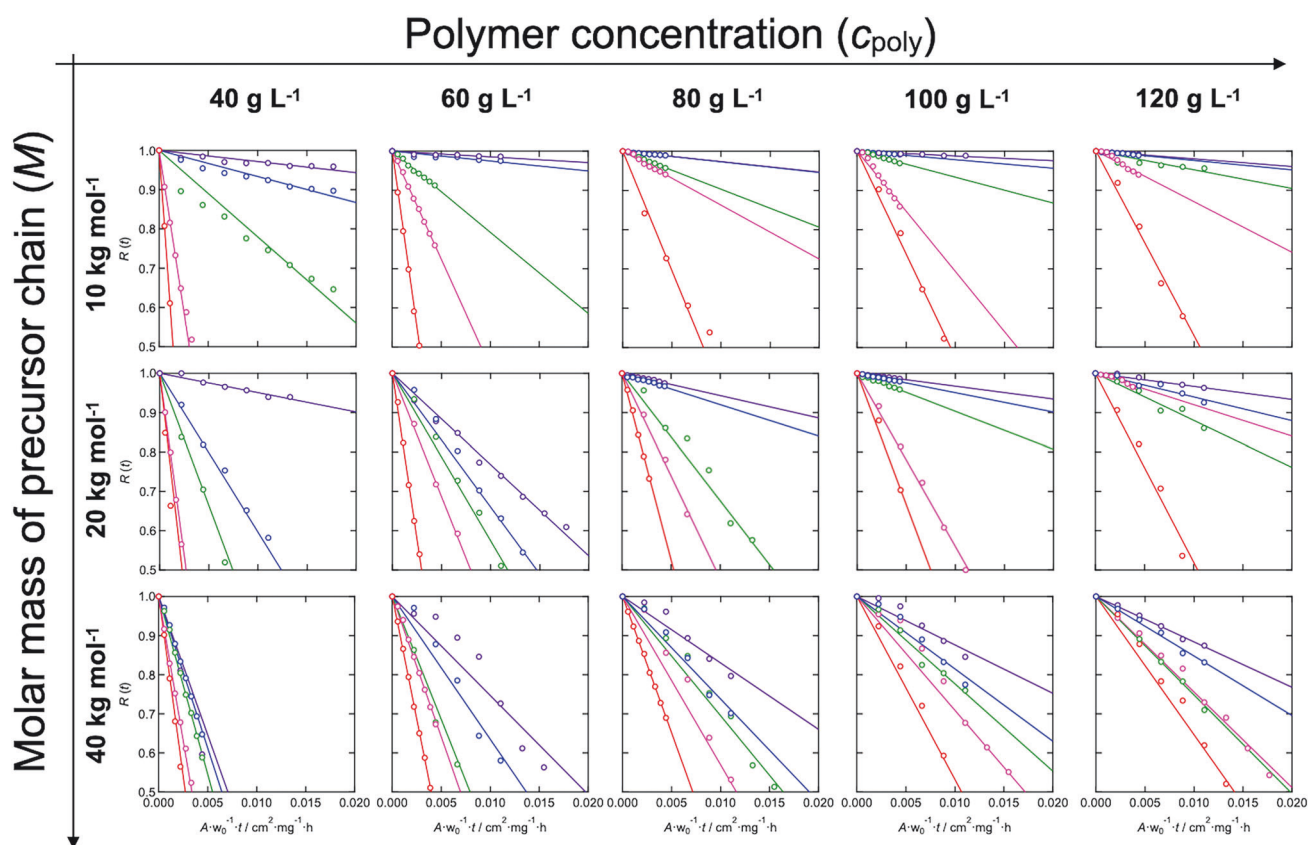
Equation (3) agrees with the results presented in Fig. 3A, B, supporting the conclusion that the dissolution of the transient network matrix governs micrometer-sized particle release. Importantly, this conclusion represents a novel finding. No previous study has demonstrated this specific combination of (1) utilizing a transient polymer network, (2) examining the release behavior of micrometer-sized particles, and (3) providing direct experimental evidence that release is controlled by matrix dissolution. This work is, therefore, the first to quantitatively establish this mechanism, setting it apart from conventional studies [28, 29], in which similar behavior may be presumed but has not been conclusively validated.

Figure 4 shows $R(t)$ as a function of time for Tetra-PEG slimes with various mixing ratios (s), polymer concentrations (c_{poly}), and molar masses of precursor chains (M) for 1 μm particles. The corresponding data for 0.1 μm particles are provided in Fig. S1 in the Supporting Information. According to Eq. (2), the time is normalized by the initial mass and surface area. The release rate increased as the mixing ratio, polymer concentration, and molar mass of the precursor chains decrease. A decrease in s and c_{poly} led to reduced elasticity in the Tetra-PEG slimes. In contrast, the elasticity increased as the molar mass of the precursor chains decreased (Fig. S2 in the Supporting Information). According to rubber elasticity theory [30–34], the elastic modulus (G) can be described by Eq. (4).

$$G = \frac{c_{poly}}{M_s} k_B T, \tag{4}$$

where M_s is the molar mass of the network strand, k_B is Boltzmann's constant, and T is the absolute temperature. Equation (4) indicates that elasticity is inversely proportional to the average network strand length. Previous studies have predicted that the diffusivity of substances in polymer networks increases with longer network strands due to the increased free volume and/or the reduced friction between the network and substances [35–37]. Our experimental results deviate from these theoretical predictions, suggesting that the interaction between the diffusive substances and the network strands does not primarily govern the release kinetics.

Figure 5 illustrates the relationship between the release constant (k) and network connectivity (p), defined as the molar fraction of bonded species relative to the total number of reactive end groups in the equilibrium state. In this study,

Fig. 3 A Residual fraction ($R(t)$) of the particles in the Tetra-PEG slimes as a function of time. The solid lines represent the fitting results obtained using Eq. (1). B Apparent release rate constant (k_{app}) as a function of the initial mass of the slimes (w_0). The solid line represents the power–law relationship of kapp vs. w_0^{-1}

polymer partially swelled due to water absorption, forming a concentration gradient and enhancing the surface polymer mobility during disentanglement. Assuming that the rate constant (k), representing the dissolution rate per unit surface area, is constant, the dissolution kinetics can be expressed by Eq. (2).

$$w_t = w_0 - k \cdot A \cdot t \tag{2}$$

where w_t and w_0 denote the matrix mass at times t and 0, respectively, and A is the surface area of the system. Notably, the slime fully covered the bottom surface of the insert and diffused in a one-dimensional manner, keeping

Fig. 4 Time-dependent residual fraction of the particles in the Tetra-PEG slimes for 1 μm particles with various connectivities, molar masses of network strands, and polymer concentrations (Purple: $s = 0.5$, blue: $s = 0.4$, green: $s = 0.36$, pink: $s = 0.33$, and red: $s = 0.3$)

p was modulated by varying the mixing ratio (s) of tetra-PEG-FPBA and tetra-PEG-GDL. The network connectivity p can be expressed by Eq. (5) [20, 38], as shown in the Supporting Information (Section 2).

$$p = \left\{ 1 + \frac{M}{4c_{poly}K} \right\} - \left[\left\{ 1 + \frac{M}{4c_{poly}K} \right\}^2 - 4s(1-s) \right]^{\frac{1}{2}}$$

(5)

where K is the equilibrium constant (500 at 25 °C, estimated from the surface plasmon resonance) [20]. Figure 5A shows the relationships between k and p. k decreased with increasing p, showing a linear relationship in the semilogarithmic plot, suggesting that k is described by an exponential function and is independent of the polymer concentration and network strand length, as depicted by the solid line. Figure 5B shows the results normalized by the release constant k_0 (the value at $p = 0$) on the vertical axis, demonstrating that all the data points lie on a single master curve. These results indicate that the release rate is monotonically constrained and delayed by network formation.

According to the Peppas model [26], the dissolution kinetics of entangled polymer networks can be classified into 2 distinct patterns. The first pattern occurs when disentanglement dominates. Under ideal sink conditions, the number of polymer chains leaving the network per unit surface area remains constant. In this case, the dissolution kinetics are determined by the characteristic disentanglement time. The second pattern is governed by the diffusion of polymers through the unstirred layer. Under ideal sink conditions, the overall dissolution rate depends on the polymer diffusivity, the concentration gradient within the unstirred layer, and the thickness and surface area of this layer. The diffusivity of the macromolecules is significantly influenced by the polymer concentration, which varies within the unstirred layer. However, once polymers enter the bulk fluid, the concentration gradient rapidly becomes linear, and the overall dissolution rate per unit surface area can be defined as a constant. In both cases, the dissolution process begins when water penetrates the polymer matrix, triggering polymer disentanglement.

The scheme proposed by Peppas [26, 27] can also be applied to transient networks with reversible bonds, where dilution reduces the binding affinity, leading to the dissolution of the constituent molecules, as described in Eq. (3). As the binding affinity decreases, the constraint strength of the network weakens, ultimately resulting in the release of particles. The release barrier for these particles depends
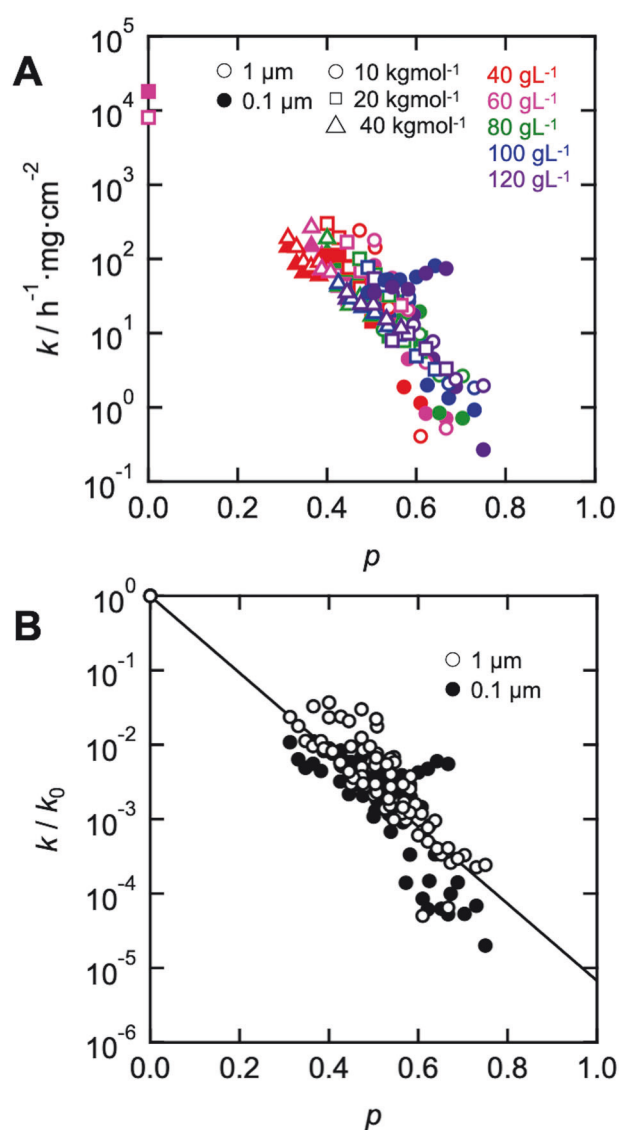
Fig. 5 A Relationships between the release constant (k) and network connectivity (p). **B** Release constant normalized by k_0 (the value at $p = 0$). The solid line represents the fitting based on the exponential function

on the topology of the surrounding network, which follows an exponential function of p, as shown in Eq. (6).

$$k = k_0 exp(-p/p_c) \qquad (6)$$

where k_0 is the release constant at a value of $p = 0$, reflecting an intrinsic characteristic of the particles. On the basis of the experimental results, the confinement parameter (p_c), which quantifies the network-induced restriction, is estimated to be approximately 0.07. This formulation represents a novel finding specific to the Tetra-PEG slime system investigated in this study. Previous studies have reported that the diffusion coefficient of particles within polymers and similar matrices decreases exponentially with increasing concentration of the surrounding matrix. The physical basis for this exponential behavior involves several

factors, including the accessibility of free volume for the particles [39–46] and variations in the activation barrier for diffusion, which are influenced by the friction and interactions between the particle and matrix [47–49]. In our case, Eq. (6) indicates that because the particles are substantially larger than the network strands, their release is governed primarily by friction with the matrix rather than by the availability of free volume. Notably, the estimated value of p_c is significantly lower than the typical percolation threshold (≈0.3 [50].) but is closer to the void percolation threshold observed in continuum models (≈0.05 [51]). This proximity implies that the release rate is governed by the probability of forming interconnected voids (pathway) within the networks, which increases as the connectivity decreases.

As noted in the introduction, our findings are limited to particles significantly larger than the network size, in which particle diffusion is negligible compared with the diffusion of the network polymers or the dynamics of dilution. If the particle size becomes comparable to or smaller than the network size, particle diffusion becomes significant, and Eq. (6) is no longer valid.

Conclusion

In this study, we experimentally investigated the effects of network structure on the release kinetics of microparticles using a model transient network (Tetra-PEG slime). The key findings are as follows: (1) the release of micrometer-sized particles is governed by the dissolution of the transient network matrix; (2) the release constant is primarily determined by the network connectivity in the equilibrium state (p) and remains largely unaffected by the polymer concentration and network strand length; and (3) the release constant follows an exponential function of p, suggesting that the probability of particles escaping the network constraints and diffusing into the external solution is regulated by the network's potential barrier associated with connectivity. These findings provide a solid foundation for the design of novel drug delivery materials that can sustainably release micron-scale entities, such as cells and viruses, from transient networks, with implications for advanced drug delivery and biomedical applications.

Data availability

The data supporting this article have been included in the main text. The raw data are available upon request to the authors.

Compliance with ethical standards

Conflict of interest The authors declare no competing interests.

References

1. Takahashi K, Yamanaka S. Induction of pluripotent stem cells from mouse embryonic and adult fibroblast cultures by defined factors. Cell. 2006;126:663–76.
2. Maude SL, Frey N, Shaw PA, Aplenc R, Barrett DM, Bunin NJ, et al. Chimeric antigen receptor T cells for sustained remissions in leukemia. N Engl J Med. 2014;371:1507–17.
3. Banchereau J, Steinman RM. Dendritic cells and the control of immunity. Nature. 1998;392:245–52.
4. Jooss K, Chirmule N. Immunity to adenovirus and adeno-associated viral vectors: implications for gene therapy. Gene Ther. 2003;10:955–63.
5. Pflepsen KR, Peterson CD, Kitto KF, Riedl MS, McIvor RS, Wilcox GL, et al. Biodistribution of adeno-associated virus serotype 5 viral vectors following intrathecal injection. Mol Pharm. 2021;18:3741–9.
6. Li J, Mooney DJ. Designing hydrogels for controlled drug delivery. Nat Rev Mater. 2016;1:16071.
7. Kharkar PM, Kiick KL, Kloxin AM. Designing degradable hydrogels for orthogonal control of cell microenvironments. Chem Soc Rev. 2013;42:7335–72.
8. Hosseinzadeh B, Ahmadi M. Degradable hydrogels: design mechanisms and versatile applications. Mater Today Sustain. 2023;23:100468.
9. Moritz S, Wiegand C, Wesarg F, Hessler N, Müller FA, Kralisch D, et al. Active wound dressings based on bacterial nanocellulose as drug delivery system for octenidine. Int J Pharm. 2014;471:45–55.
10. Trovatti E, Freire CSR, Pinto PC, Almeida IF, Costa P, Silvestre AJD, et al. Bacterial cellulose membranes applied in topical and transdermal delivery of lidocaine hydrochloride and ibuprofen: in vitro diffusion studies. Int J Pharm. 2012;435:83–87.
11. Winter HH, Chambon F. Analysis of linear viscoelasticity of a crosslinking polymer at the gel point. J Rheol. 1986;30:367–82.
12. Martin JE, Wilcoxon JP. Critical dynamics of the sol–gel transition. Phys Rev Lett. 1988;61:373–6.
13. Lyu Y, Azevedo HS. Supramolecular hydrogels for protein delivery in tissue engineering. Molecules. 2021;26:873.
14. Saunders L, Ma PX. Self-healing supramolecular hydrogels for tissue engineering applications. Macromol Biosci. 2019;19:e1800313.
15. Katashima T. Molecular understanding of viscoelasticity in transient polymer networks based on multiple methods. Nihon Reoroji Gakkaishi. 2022;50:51–56.
16. Shibayama M. Spatial inhomogeneity and dynamic fluctuations of polymer gels. Macromol Chem Phys. 1998;199:1–30.
17. Katashima T. Rheological studies on polymer networks with static and dynamic crosslinks. Polym J. 2021;53:1073–82.
18. Katashima T. Precise rheological analysis of permanently and transiently crosslinked polymer networks with well-controlled structures. Nihon Reoroji Gakkaishi. 2023;51:273–80.
19. Michida S, Chung U-I, Katashima T. Probing the molecular mechanism of viscoelastic relaxation in transient networks. Gels. 2023;9:945.
20. Katashima T, Kudo R, Naito M, Nagatoishi S, Miyata K, Chung U-I, et al. Experimental comparison of bond lifetime and viscoelastic relaxation in transient networks with well-controlled structures. ACS Macro Lett. 2022;11:753–9.
21. Parada GA, Zhao X. Ideal reversible polymer networks. Soft Matter. 2018;14:5186–96.
22. Marco-Dufort B, Iten R, Tibbitt MW. Linking molecular behavior to macroscopic properties in ideal dynamic covalent networks. J Am Chem Soc. 2020;142:15371–85.
23. Yesilyurt V, Webber MJ, Appel EA, Godwin C, Langer R, Anderson DG. Injectable self-healing glucose-responsive hydrogels with pH-regulated mechanical properties. Adv Mater. 2016;28:86–91.
24. Yesilyurt V, Webber MJ, Appel EA, Godwin C, Langer R, Anderson DG. Mixed reversible covalent crosslink kinetics enable precise, hierarchical mechanical tuning of hydrogel networks. Adv Mater. 2017;29:1605943.
25. Matsumoto A, Ishii T, Nishida J, Matsumoto H, Kataoka K, Miyahara Y. A synthetic approach toward a self-regulated insulin delivery system. Angew Chem Int Ed Engl. 2012;51:2124–8.
26. Siepmann J, Kranz H, Bodmeier R, Peppas NA. HPMC-matrices for controlled drug delivery: a new model combining diffusion, swelling, and dissolution mechanisms and predicting the release kinetics. Pharm Res. 1999;16:1748–56.
27. Peppas NA, Wu JC, von Meerwall ED. Mathematical modeling and experimental characterization of polymer dissolution. Macromolecules. 1994;27:5626–38.
28. Aibara S, Yoshida R, Miyamoto M, Kokufuta E, Ito K, Mayumi K. Structure and dynamics of Tetra-PEG gels with controlled network defects. Biomacromolecules. 2020;21:4391–4400.
29. Noro A, Hayashi K, Matsushita Y, Matsuba G, Ito K. Diffusion of star polymers through a permanently cross-linked polymer network. Langmuir. 2020;36:5205–11.
30. Flory PJ, Rehner J Jr. Statistical mechanics of cross-linked polymer networks I. rubberlike elasticity. J Chem Phys. 1943;11:512–20.
31. Treloar LRG. The elasticity of a network of long-chain molecules. I. Trans Faraday Soc. 1943;39:36.

32. Treloar LRG. The elasticity of a network of long-chain molecules.—III. Trans Faraday Soc. 1946;42:83–94.

33. Treloar LRG. The elasticity of a network of long-chain molecules—II. Trans Faraday Soc. 1943;39:241–6.

34. Wall FT. Statistical thermodynamics of rubber. II. J Chem Phys. 1942;10:485–8.

35. Masaro L, Zhu XX. Physical models of diffusion for polymer solutions, gels and solids. Prog Polym Sci. 1999;24:731–75.

36. Peppas NA, Reinhart CT. Solute diffusion in swollen membranes. Part I. A new theory. J Memb Sci. 1983;15:275–87.

37. Reinhart CT, Peppas NA. Solute diffusion in swollen membranes. Part II. Influence of crosslinking on diffusive properties. J Memb Sci. 1984;18:227–39.

38. Katashima T, Kimura T, Sugawara K, Chung U-I, Sakai T. Effects of network connectivity on viscoelastic relaxation in transient networks using experimental approach. Front Soft Matter. 2022;2:1059156.

39. Hedenqvist M. Diffusion of small-molecule penetrants in semi-crystalline polymers. Prog Polym Sci. 1996;21:299–333.

40. Stern SA, Sampat SR, Kulkarni SS. Tests of a 'free-volume' model of gas permeation through polymer membranes. II. Pure Ar, SF6, CF4, and C2H2F2 in polyethylene. J Polym Sci B Polym Phys. 1986;24:2149–66.

41. Kulkarni SS, Stern SA. The diffusion of CO2, CH4, C2H4, and C3H8 in polyethylene at elevated pressures. J Polym Sci Polym Phys Ed. 1983;21:441–65.

42. Zhu XX, Wang F, Nivaggioli T, Winnik MA, Macdonald PM. Poly(methyl methacrylate) film dissolution and solvent diffusion coefficients: correlations determined using laser interferometry-fluorescence quenching and pulsed-gradient spin-echo NMR spectroscopy. Macromolecules. 1993;26:6397–402.

43. Zhu XX, Macdonald PM. Pulsed-gradient spin-echo NMR measurements of the diffusion coefficients of ketones in poly(methyl methacrylate). Macromolecules. 1992;25:4345–51.

44. Xia J, Wang CH. Holographic grating relaxation studies of probe diffusion in amorphous polymers. J Polym Sci B Polym Phys. 1995;33:899–908.

45. Kim D, Caruthers JM, Peppas NA, von Meerwall E. Self- and mutual-diffusion coefficients in the dodecane/polystyrene system. J Appl Polym Sci. 1994;51:661–8.

46. Bandis A, Inglefield PT, Jones AA, Wen W-Y. A nuclear magnetic resonance study of dynamics in toluene-polyisobutylene solutions: 1. Penetrant diffusion and Fujita theory. J Polym Sci B Polym Phys. 1995;33:1495–503.

47. Gao P, Fagerness PE. Diffusion in HPMC gels. I. Determination of drug and water diffusivity by pulsed-field-gradient spin-echo NMR. Pharm Res. 1995;12:955–64.

48. Pickup S, Blum FD. Self-diffusion of toluene in polystyrene solutions. Macromolecules. 1989;22:3961–8.

49. Nyström B, Moseley ME, Brown W, Roots J. Molecular motion of small molecules in cellulose gels studied by NMR. J Appl Polym Sci. 1981;26:3385–93.

50. Xu X, Wang J, Lv JP, Deng Y. Simultaneous analysis of three-dimensional percolation models. Front Phys. 2014;9:113–9.

51. Xu Y, Li Q, King HE. Modeling oil recovery for mixed macro- and micro-pore carbonate grainstones. Sci Rep. 2017;7:9780.